SAND2000-1037J

Integrated Experimental and Computational Methods for Structure Determination and Characterization of a New, Highly Stable Cesium Silicotitanate Phase, $Cs_2TiSi_6O_{15}$ (SNL-A)

M. Nyman[§], F. Bonhomme[§], D. M. Teter[£], R. S. Maxwell[¶], B. X. Gu[†], L. M. Wang[†], R. C. Ewing[†], and T. M. Nenoff[§]*.

[§]Catalysis and Chemical Technologies Department, M.S. 0710
[£]Geochemistry Department, M.S. 0750
Sandia National Laboratories, P.O. Box 5800, Albuquerque, NM 87185

[¶]Lawrence Livermore National Laboratory, Analytical and Nuclear Sciences Division
P.O. Box 808/L-091, Livermore, CA 94551

[†]Department of Nuclear Engineering and Radiological Sciences, University of Michigan,
Ann Arbor, MI 48109-2104.

*Author to whom correspondence should be addressed.

Abstract

Exploratory hydrothermal synthesis in the system Cs_2O-SiO_2-TiO_2-H_2O has produced a new polymorph of $Cs_2TiSi_6O_{15}$ (SNL-A) whose structure was determined using a combination of experimental and theoretical techniques (^{29}Si and ^{133}Cs NMR, X-ray Rietveld refinement, and Density Fuctional Theory). SNL-A crystallizes in the monoclinic space-group *Cc* with unit cell parameters: a = 12.998 (2) Å, b = 7.5014 (3) Å, c = 15.156 (3) Å, β = 105.80 (3)°. The SNL-A framework consists of silicon tetrahedra and titanium octahedra which are linked in 3-, 5-, 6-, 7- and 8-membered rings in three dimensions. SNL-A is distinctive from a previously reported *C2/c* polymorph of $Cs_2TiSi_6O_{15}$ by different ring geometries. Similarities and differences between the two

structures are discussed. Other characterizations of SNL-A include TGA-DTA, Cs/Si/Ti elemental analyses, and SEM/EDS. Furthermore, the chemical and radiation durability of SNL-A was studied in interest of ceramic waste form applications. These studies show that SNL-A is durable in both radioactive and rigorous chemical environments. Finally, calculated cohesive energies of the two $Cs_2TiSi_6O_{15}$ polymorphs suggest that *Cc* SNL-A phase (synthesized at 200 °C) is energetically more favorable than the *C2/c* polymorph (synthesized at 1050 °C).

Introduction

We are currently studying the viability of silicotitanate phases for cleanup of radionuclides such as ^{90}Sr and ^{137}Cs. Silicotitanate materials of interest include: (1) microporous phases for radionuclide sorption, and (2) condensed, leach resistant phases for radionuclide storage. The ^{137}Cs and ^{90}Sr together compose greater than 99 % of the radioactive inventory of the Hanford wastes, and removal and immobilization of these radionuclides is a primary goal for remediation of this DOE defense waste site.[1,2] A proprietary ion exchanger material jointly developed by Sandia National Laboratories and Texas A & M University, designated crystalline silicotitanate (CST), is currently the best candidate for ^{137}Cs removal.[3-6] Furthermore, its oxide components are suitable for the matrix of a ceramic waste from. Heat treating Cs-loaded CST up to 1000 °C results in dehydration and subsequent formation of a mixture of crystalline phases which are very resistant to Cs leaching.[7,8] With the interest of studying the unique durability and stability of silicotitanate phases, a collaborative effort between Sandia National Laboratories (SNL) (hydrothermal synthesis and characterization), Pacific Northwest National Laboratory (PNNL) (solid state synthesis and characterization), and U. C. Davis (calorimetry studies[9] is ongoing to carry out phase searches using component oxides of the Cs-loaded CST material. Current investigations include hydrothermal and solid-state synthesis of ternary Cs_2O-SiO_2-TiO_2-H_2O phases.

Prior to this collaboration, only one ternary Cs_2O-SiO_2-TiO_2-H_2O phase had been reported. This phase is a Cs/Si/Ti pharmacosiderite analogue, $HCs_3Ti_4Si_3O_{16}\bullet 4H_2O$, which is a hydrothermally-synthesized, microporous ion exchanger.[10,11] The efforts of this study have added four additional Cs_2O-SiO_2-TiO_2 phases which include: a) Phases synthesized by solid-state/flux routes at PNNL, $CsTiSi_2O_{6.5}$ (pollucite analogue) and the *C2/c* polymorph of $Cs_2TiSi_6O_{15}$ [12-15] and b) Phases synthesized by hydrothermal routes at SNL, microporous $Cs_3TiSi_3O_{9.5}\bullet 3H_2O$ (SNL-B) [16,17] and the currently reported *Cc* polymorph of $Cs_2TiSi_6O_{15}$ (SNL-A).

The synthesis, structure determination and characterization of the *Cc* polymorph of $Cs_2TiSi_6O_{15}$ is presented in this report. The focus of this body of work is four-fold: 1) hydrothermal synthesis of a new ternary Cs_2O-SiO_2-TiO_2 phase, 2) the integrated use of three techniques (X-ray Rietveld refinement, Density Functional Theory (DFT), and ^{29}Si and ^{133}Cs solid-state NMR) to determine the correct structure of a complex microcrystalline powder phase with 24 independent atoms in the unit cell, 3) comparison of the structure, stability, physical properties and synthesis conditions of *Cc* SNL-A to the *C2/c* polymorph, and 4) examination of the theoretical, chemical and radiation stability of SNL-A, to assess its viability as a waste form phase.

Experimental

General Instrumentation. The **X-ray powder diffraction** pattern of $Cs_2TiSi_6O_{15}$ was measured on a Siemens D500 diffractometer with a Ni-filtered CuKα radiation. The data were collected over the angular range 5-100 ° 2θ with a step size of 0.025 ° and a counting time of 20 seconds per step. The front-loaded sample was rotated at 30 rpm during the measurement. **Magic Angle Spinning Nuclear Magnetic Resonance Spectrometry**: The ^{133}Cs MAS NMR was acquired at 65.6 MHz (11.7T) on a Bruker DRX-500 spectrometer using a Bruker 4 mm CP MAS probe. Sample spinning speed was kept constant at 10 kHz. The ^{133}Cs spectrum was recorded at both fields using a 1-pulse acquire experiment with proton decoupling. Pulse lengths were chosen to be approximately 1/4th of a non-selective $\pi/2$ (~8 μs), though experiments with variable pulse lengths indicated that all peaks could be characterized by the same nutation behaviour. Solid cesium chloride and 0.1 M CsCl (0 ppm) were used for external standardization. A 300 second recycle delay was used, and 192 scans were collected. The ^{29}Si MAS NMR was performed at 99.4 MHz on the same Bruker DRX-500 spectrometer and 4 mm probe. The ^{29}Si MAS NMR spectrum was also acquired with 1-pulse acquire experiments though full nonselective $\pi/2$ pulses of 8.5 μs were used. Neat tetramethylsilane (TMS) was used as an external standard (0 ppm) for the ^{29}Si NMR. A recycle delay of 600 seconds was used, and 400 scans were collected. **Inductively Coupled Plasma Spectroscopy (ICP)** for Si and Ti was carried out using an AtomScan-25 ICP-AES instrument, with an argon plasma flame. Samples were dissolved in HF and diluted with water. Reference samples were 10 ppm Si and Ti. Elemental analysis for Cs by **Atomic Adsorption Spectroscopy (AAS)** was performed on a Perkin Elmer 5100 PC AAS instrument. Solutions and standards were prepared with 1000 ppm ionization suppressant. An acetylene/air flame was used for Cs analysis. The **Differential Thermal Analysis-Thermogravimetric Analysis (DTA-TGA)** experiments were performed on a STD 2960 TA DTA-TGA instrument with alumina as a standard for DTA. Samples of SNL-A (10 - 15 mg) were heated at 5 °C/min to 1400 °C with an argon flow of 20 cc/min. **Scanning Electron Microscopy (SEM)** data is collected on a JEOL JSM-T300 SEM with energy dispersive capabilities. **BET surface area** measurements were performed on a Quantachrome Autosorb 6B automated gas sorption system, with adsorbed and desorbed volumes of nitrogen at relative pressures in the range 0.05 to 1.0.

Synthesis of SNL-A. Titanium isopropoxide (TIPT, 0.64 mmol) and tetraethylorthosilicate (TEOS, 5.1 mmol) were combined by stirring and added dropwise to 50% CsOH solution (5.1 mmol) in a 23 ml teflon liner for a Parr pressure reactor. After stirring for approximately 30 minutes, 7.3 mL H_2O was added and the mixture was stirred for 30 minutes more. The final pH of the mixture was approximately 12.7 with a final stoichiometry of $Cs:Ti:Si:H_2O = 8:1:8:695$. The Parr pressure reactor was placed in a 200 °C oven and heated for two weeks. The product was collected by filtration and washed with hot deionized water.

Cesium Leach Tests. The standard PCT (product consistency test) leach test, a common technique developed to evaluate chemical durability of nuclear waste forms in aqueous environments[18,19], was performed on SNL-A. A sample of the material (0.2 g) was placed in a hydrothermal bomb with 10 grams of water at 90 °C for 1, 2, 3, 7, and 10 days. After the designated time of heating, each sample was filtered and the leachate solution was analyzed for Cs concentration by AAS. The solid product was analyzed by XRD to determine if any phase changes had occurred. Surface area of samples for leach rate calculations was determined by BET measurements (29 m^2/g).

Electron Irradiation Studies. Electron irradiation studies of SNL-A were conducted with a JEOL 2000FX transmission electron microscope (TEM) at the University of Michigan. The electron energy used was 200 keV and the sample was irradiated at a dose rate of 5×10^{23} electrons / s•cm^2.

Results and Discussion

Synthesis and Bulk Characterizations of SNL-A. Approximately 0.3 g (0.42 mmol) of SNL-A is collected from the synthesis reaction described above. This corresponds with a 66 % yield based on TIPT, the limiting reagent in the synthesis reaction. The reaction is also directly scaleable to obtain more product per synthesis, by utilizing a larger Parr pressure reactor (125 ml teflon liner). Wet chemical analysis for concentrations of Ti (ICP), Si (ICP) and Cs (AA) gave 24.5 wt % Si (calc. 23.3 wt %), 6.77 wt % Ti (calc. 7.25 wt %) and 38.3 wt % Cs (calc. 36.8 wt %). Within experimental error of the analysis techniques (approximately ± 5 %), the product is pure with the stoichiometry $Cs_2TiSi_6O_{15}$. This stoichiometry is also determined by EDS/SEM analysis for Cs, Si and Ti. SNL-A as viewed by SEM is shown in figures 1a and 1b. Figure 1a (1000x magnification) shows the uniformity of the crystallite size and the purity of the sample. Figure 1b (3500x magnification) shows the irregular shape of the crystallites, which are approximately 2 – 5 microns in diameter. No other phases are observed by SEM, which lends further evidence to the formation of a pure material.

Analysis by DTA-TGA reveals a weight loss of less than 1% upon heating to 1400 °C, which indicates SNL-A contains no volatile components such as water molecules or hydroxyl ions. No phase changes are observed by DTA, except an endothermic melting at 1150 °C, which is the same melting temperature observed for the PNNL *C2/c* polymorph of $Cs_2TiSi_6O_{15}$[20]. Upon melting, SNL-A does not recrystallize. Rather, it solidifies as a glassy material. Furthermore, SNL-A does not undergo any solid-state phase transformations up to its melting point, which suggests it is extremely stable. Additionally, SNL-A heated at 1000 °C for 8 hours did not show any change in its X-ray diffraction pattern.

The PNNL *C2/c* polymorph is synthesized by either high temperature (1050 °C) solid-state reactions of cesium nitrate, titania and silica [20], or grown from the $CsTiSi_2O_{6.5}$ pollucite analogue as a precursor in a cesium vanadate flux at 1100 °C.[14] The SNL-A phase has thus far only been synthesized hydrothermally at 120 – 250 °C. However, since SNL-A cannot be converted to the PNNL phase, the two polymorphs cannot be considered high and low temperature forms. In this study, the energetics of the two phases are compared by DFT total energy calculations (discussed below) Furthermore, calorimetry studies on the two $Cs_2TiSi_6O_{15}$ polymorphs are currently being carried out with Navrotsky et al., and will give more insight into the relative stability of these phases.

Structure Determination and Refinement. Since no single crystal of sufficient size could be grown, the structure of SNL-A had to be solved *ab-initio* from X-ray powder diffraction data. Powder X-ray diffraction data was collected as described above. From that data, the positions of the first 20 Bragg peaks (corrected with Si as external standard) were used for the indexation with the programs TREOR90[21] and DICVOL91[22]. A satisfactory solution was found in the monoclinic system with approximate cell parameters a = 12.97 Å, b = 7.50 Å, c = 15.15 Å and β=105.70 °, which is similar to those reported for the PNNL phase (a = 13.386(5) Å, b= 7.423(3) Å, c = 15.134(5) Å, β = 107.71(3)° [14]). The extinction laws were consistent with the space-groups *Cc* or *C2/c*. The number of independent Cs and Si sites revealed by the NMR data was only consistent with a structure described in the non centrosymmetric group *Cc*. The correctness of the cell and space group extinctions were checked by a full pattern fitting using the Le Bail method[23], as implemented in the program FULLPROF[24]. No peak was left unaccounted for, thus establishing the validity of the cell and the purity of the sample. The extracted integrated intensities of the peaks below $2\theta = 50°$ were used to solve the structure in the space group *Cc* by direct methods with the program SIR92[25], incorporated in the Wingx[26] suite.

The positions of the cesium atoms and of several of the non-oxygen atoms were directly revealed. The correct assignment of atom types and the completion of the structure were achieved by successive Rietveld refinement using the WinMprof program[27], difference Fourier analysis and "manual" model-building. Although the framework characteristics and topology of the fully refined structure appeared to be essentially correct, the completely free Rietveld refinement of the 70 free atomic positional parameters led to an *unreasonably broad range of Si-O distances*, with a mean value of 1.59 Å and a standard error of 0.13 Å. This imprecision on the oxygen atom positions is partly due to the relative complexity of the structure (24 independent atoms and 70 free positional parameters) and to the strong scattering of the cesium atoms, which tend to overwhelm the contribution of the Si-Ti-O framework. Furthermore, the positions of the non-oxygen atoms can be well described in the centrosymmetric space-group *C2/c* (program MISSYM[28]). About two thirds of the scattering power of the cell are thus related by a pseudo center of symmetry, which tends to introduce high correlation between refined parameters.

In order to obtain a more reasonable structure in the correct (*Cc*) than that achieved by the original free Rietveld refinement as described above, two different approaches were used. The first approach was a Rietveld refinement with soft constraints applied on all 24 independent Si-O distances (Si-O = 1.60 (2) Å). This constrained refinement of the atomic and profile parameters (91 parameters all together) proceeded smoothly down to very satisfactory agreement indices (R_{Bragg}= 3.37%, R_p= 11.73%, χ^2=7.62). No preferred orientation correction was necessary. The Cs sites are fully occupied and no disorder on the Si/Ti sites is evidenced. In comparison with the free refinement, the average shift of the Ti/Si and O atoms from their original positions are 0.05 Å and 0.12 Å respectively, and the Cs atoms are essentially unshifted.

The second approach used was to optimize the atomic coordinates by minimizing the energy of the structure. This work was carried out by Density Function Theory (DFT) using the VASP code developed at the Institut fur Theoretische Physik of the Technische Universitat Wien.[29-32] The quantum mechanical modeling of $CsTi_2Si_6O_{15}$ is a computationally demanding task. The problems of deep pseudopotentials required to accurately model the oxygen ion, combined with the low symmetry and large unit cell would have made these calculations intractable until recently.

The electronic degrees of freedom were minimized using a residual minimization method direct inversion in the iterative subspace (RMM-DIIS) algorithm.[33,34] The program solves for the electronic charge density using a density functional framework[35,36] within the local density approximation to electron exchange and correlation. The exchange correlation term of the total energy is the Perdew and Zunger parameterization[37] of the Ceperley and Alder data[38]. The electronic wave functions are expanded in a plane wave basis set with periodic boundary conditions. Vanderbilt ultrasoft pseudopotentials were used for the cesium, titanium and oxygen ions with the following states being treated as valence electrons: Cs:$5p^6$ $6s^1$, Ti: $3p^6$ $3d^2$ $4s^2$, and O:$2s^2$ $2p^4$. A norm-conserving pseudopotential was used for silicon with the $3s^2$ $3p^2$ states being treated as valence. The internal coordinates of the initial unit cell derived from the free Rietveld refinement were optimized while keeping the unit cell and cesium ions fixed because of the very low experimental uncertainties on these structural constraints (R_{Bragg}=3.20%). These calculations resulted in optimization of the framework atoms to obtain the most reasonable Si-O/Ti-O bond distances of the three models.

Table 1 shows a comparison of agreement indices for the three models: 1) free Rietveld refinement, 2) Rietveld refinement with Si-O constraint, 3) DFT structural optimization with Cs and unit cell fixed. Although the free Rietveld refinement gave the best agreement indices due to the greatest degrees of freedom on the model, this data set is disregarded for the remainder of the discussion, due to the unreasonable Si-O distances. The crystallographic data and refinement conditions for the "distance constrained" refinement are presented in Table 2; and the observed, calculated and difference plots for this model are shown in figure 2. The structural parameters for two models are given in Table 3: 1) Rietveld refinement with Si-O constraint, and 2) DFT structural optimization with Cs position and cell parameters fixed. Although atomic positions are very similar for both models, the DFT model gave a more reasonable range of Ti-O distances (1.917 – 1.976 Å) than the Rietveld model with Si-O constraint (1.84 (3) – 2.08 (3) Å). Selected interatomic distances and bond angles from the Rietveld model with Si-O constraint are given in Table 4.

Description of Framework. The composition and melting temperature are identical for SNL-A and the PNNL phase, and the unit cell parameters are quite similar. The calculated powder diffraction patterns of SNL-A and the PNNL phase are shown in figure 3 for comparison. The differences between the diffraction patterns are apparent, confirming there are two distinct polymorphs of $Cs_2TiSi_6O_{15}$. Furthermore, there are distinct differences in the polyhedral rings which make up the silicotitanate framework. SNL-A has six crystallographically unique Si sites, 1 unique Ti site and two unique Cs sites. The PNNL phase is of higher symmetry with 3 unique Si sites, 1 unique Ti site and 1 unique Cs site. For both phases, all TiO_6 octahedra share six corners with SiO_4 tetrahedra, and each SiO_4 tetrahedron is linked to one TiO_6 octahedron and three other SiO_4 tetrahedra. The polyhedra form 3-, 5-, 6-, 7- (SNL-A only) and 8- membered rings that comprise channels in which the cesium cations reside. The ring types which are found in the PNNL and SNL-A phases are summarized in Table 5 for comparison, where Ti is a TiO_6 octahedron, Si(n) is a SiO_4 tetrahedron and $Si(n)_2$ is a Si_2O_7 (n = 1 - 3). The major difference between the two polymorphs is the 7- and 8-membered rings. The PNNL phase has two types of 8-membered rings; one with all SiO_4 tetrahedra and one with 6 SiO_4 tetrahedra and 2 TiO_6 octahedra. SNL-A has only the SiO_4 tetrahedra 8-membered ring, and a unique 7-membered ring (which is not observed in the PNNL phase).

SNL-A viewed down the *a*-axis is shown in figure 4. This projection clearly shows undulating layers of Si_2O_7 [Si(3)-Si(6) and Si(1)-Si(2)] units alternating with layers of titanium octahedra, parallel to the *b*-axis. This view also emphasizes the 5-membered rings composed of four SiO_4 tetrahedra and one TiO_6 octahedron. The 6-membered rings observed in this view are made up of 4 SiO_4 tetrahedra and 2 TiO_6 octahedra. This is a similar view observed in the PNNL phase projected down the *b*-axis.[14]

A view approximately down the (011) axis of SNL-A is shown in figure 5, which is most similar to the (101) view of the PNNL phase.[14] This view reveals the major differences between SNL-A and the PNNL phase. In this projection, an 8-memebered ring, a 7-membered ring and a 3-membered ring are observed. The 3-membered ring consists of one TiO_6 octahedron, an $Si(1)O_4$ and an $Si(3)O_4$ tetrahedron; this 3-membered ring is also present in the PNNL phase. The 8-membered ring consists of eight silicon tetrahedra. The 7-membered ring is not observed in the PNNL phase. Instead, the PNNL phase has a second 8-membered ring consisting of 2 TiO_6 octahedra and 6 SiO_4 tetrahedra. The Cs atoms are located within the 7-membered ring and 8-membered ring channels which run approximately perpendicular to the view shown in figure 5. The shortest Cs-Cs distances are observed within these channels. Cs2 and Cs1 alternate with slightly varying distances of 4.685 (2) Å, 5.105 (2) Å and 4.679 (2) Å. In comparison, the shortest Cs-Cs distances reported for the PNNL phase are 3.765 (2) Å and 4.904 (2) Å.

A second type of 5-ring consisting of 5 SiO_4 tetrahedra is approximately perpendicular to the 8-silicon ring. Both the 5-membered SiO_4 ring and 8-membered SiO_4 ring are emphasized in the view (approximate (101) plane) in figure 6. The 5-membered SiO_4 ring layers alternate with the 8-membered SiO_4 ring layers in a stair-step fashion. A 5-membered SiO_4 ring is also present in the PNNL phase.

^{29}Si and ^{133}Cs MAS NMR. Solid state ^{29}Si and ^{133}Cs MAS NMR analyses of a pure sample of SNL-A gave 6 peaks (~1:1:1:1:1:1 ratio) and 2 peaks (1:1 ratio), respectively. These results played a pivotal role in the final solving and refinement of the structure in the *Cc* space group rather than *C2/c* space group (which has 3 Si and 1 Cs per unit cell). The ^{29}Si and ^{133}Cs NMR plots are shown in figures 7a and 7b, respectively. The ^{29}Si chemical shifts observed for six unique sites range from –96.8 to –110.0 ppm, which is an unusually large shift range for all Q^3 sites (3Si, 1Ti). Furthermore, by conventional Q^x peak assignments, the peak at –110.0 ppm is usually assigned the Q^4 designation.[39] Given these unusual features of the NMR data and the important role the NMR data served in the structure determination, we calculated ^{29}Si shifts using empirical equations first reported by Sherriff[40] and later used specifically for silicotitanates by Labouriau[41].

The ^{29}Si peak shifts were calculated using both data sets: 1) the Rietveld refinement with Si-O constraint and 2) the DFT optimization with Cs and unit cell fixed. These results, along with key structural parameters in the equations, namely the Si(x)-O-Si average bond angle and Si(x)-O-Ti bond angle (x = 1 - 6) are summarized in Table 6. In general, the down field shift increases with increasing average Si(x)-O-X (X=Si, Ti) angle, especially the average Si(x)-O-Si bond angle. The data from the DFT model gave calculated chemical shifts which agree very well with the observed shifts, and the peaks were assigned to crystallographic sites based on this data (see Table 6, column 1). Finally, both sets of calculated ^{29}Si peak shifts show that the large chemical shift range observed for chemically similar (Q^3, 3Si, 1Ti) sites is expected, based on the large range of Si-O-X (X=Si, Ti) bond angles within the framework of SNL-A.

The ^{133}Cs MAS NMR spectrum (figure 7b) shows two unique chemical sites in a 1:1 ratio, which also agrees with the crystallographic data. Figure 8 shows the chemical environments of Cs1 and Cs2, out to the first oxygen coordination spheres. The Cs1 is surrounded by 12 oxygen atoms in the first coordination sphere, and the average Cs-O distance is 3.5 Å. The Cs2 is surrounded by 13 oxygen atoms in the first coordination sphere, and the average Cs-O distance is 3.4 Å. The ^{133}Cs NMR chemical shifts are affected by shielding of the Cs by neighboring atoms; where in general, down field shifts correlate with decreased shielding.[42-44] This suggests the peak at 69.4 ppm corresponds with the Cs2 which has longer Cs-O distances and the peak at 91.8 ppm corresponds the Cs1 with shorter Cs-O bond distances.

Stability of SNL-A. Described below is a summary of experiments executed to determine the energetic stability, and the chemical and radiation stability of SNL-A. These experiments were carried out to investigate the viability of SNL-A as a ceramic waste form phase, such as that which might be formed by thermal conversion of a Cs-exchanged silicotitanate ion exchanger.

Energetics of SNL-A. Using DFT total energy calculations, we optimized the positions of all the ionic coordinates and the shape of the unit cell as a function of volume in order to compare the energetics of the *Cc* and *C2/c* model solutions for SNL-A and that of the PNNL phase. At a given volume, the positions of the cations and the anions were determined by minimizing the Hellmann Feynman forces on the ions. The unit cell edges were determined by making adjustments, until the Pulay corrected stress tensor was zero. The structural parameters were considered to be fully relaxed when the forces on the ions were less that 0.005 eV/A and all stress tensor components were less than 0.001 eV/A^3. Calculations of this type were completed for a variety of volumes for each structure type. The resulting energies were fit to a Birch[45] equation of state

$$E= a_0 + a_1V^{-2/3} + a_2V^{-4/3} + a_3V^{-6/3} \quad (1)$$

which was used to determine the pressure, the bulk modulus (B_0), and the pressure derivative of the bulk modulus (B'_0). In order to estimate with some degree of confidence the small energy differences between these structures, a kinetic energy cutoff of 500 eV was used. The Brillouin zone integration was completed using a [222] Monkhorst-Pack type grid which reduced to 3 *k*- points in the irreducible Brillouin zone.[46-48] The results of these calculations are shown in the plot in figure 9. These results shows that the *Cc* solution is energetically favorable to the *C2/c* solution for SNL-A. In agreement with the NMR data and Rietveld refinement data, these calculations lended further evidence for the *Cc* model as the correct structure for SNL-A. Finally, the cohesive energy of SNL-A is found to be lower (higher stablility) than the PNNL *C2/c* polymorph.

Chemical durability of SNL-A. SNL-A shows extreme durability in aggressive chemical and radiation environments. The durability of SNL-A with respect to Cs leachability is shown in figure 10, where leach rate is plotted as a function of leach time. Less than 0.2% Cs is lost from the original 37% by weight Cs composition, which translates as essentially no Cs lost due to leaching. Furthermore, SNL-A did not undergo any phase change as a result of the PCT leach tests, as determined by powder X-ray analysis of the leached samples. Furthermore, attempted ion exchange experiments (3 days at 90 °C) in: 1) one molar aqueous sodium chloride solution, and 2) one molar aqueous sodium hydroxide solution, resulted in no ion exchange and no structural change.

Radiation durability of SNL-A . Radiation stability determination of all Cs silicotitanate phases synthesized in the collective (SNL/PNNL/U.C. Davis) studies is important in order to assess the durability of the phases for ion exchange with radionuclides or waste form applications. Electron irradiation with *in situ* TEM studies have proven to be useful in simulating the effects of radiation damage caused by fission products.[16,49,50] SNL-A is extremely radiation resistant. Figure 11 shows the electron diffraction pattern of SNL-A, before and after cumulative radiation dose of 5 x 10^{23} electrons/cm^2. No changes in the diffraction pattern resulting from irradiation induced amorphization are observed.

Summary and Conclusions

Ternary phase searches by hydrothermal treatment (120 – 200 °C) of Cs_2O-SiO_2-TiO_2-H_2O precursor mixtures has produced a new *Cc* polymorph of $Cs_2TiSi_6O_{15}$ (SNL-A). SNL-A is stable up to its melting temperature at 1150 °C; upon cooling, a glass is formed. No interconversion between the *Cc* –SNL-A and *C2/c* -PNNL polymorphs are observed. The two polymorphs are similar in their unit cell dimensions and identical in melting temperature. However, distinctions are seen in the ring structures. SNL-A possesses a 7-membered ring which is not observed in the *C2/c* -PNNL polymorph, and the *C2/c* -PNNL polymorph has an 8-membered ring which is not found in SNL-A.

The structure of SNL-A is approximately centrosymmetric; the Rietveld refinement of SNL-A powder X-ray diffraction data provided a satisfactory model in the space group *C2/c*. However, both ^{133}Cs and ^{29}Si MAS NMR spectroscopy suggested twice as many unique crystallographic sites for Cs and Si than this solution predicted. DFT total energy calculations were applied to optimize both the *Cc* and *C2/c* model structures. The DFT total energy calculations showed the cohesive energy for the *Cc* solution for SNL-A to be lower than that of the *C2/c* solution, which again suggests the *Cc* solution is correct. This approach gave a solution with better agreement indices, and which agreed with the NMR data. Calculations of theoretical ^{29}Si NMR chemical shifts for SNL-A using both the DFT and Rietveld refinement results showed that the down field chemical shift increases with increasing Si-O-X angle, where X is the neighboring Si or Ti. The chemical shifts calculated from the DFT data agree better with the observed shifts than those calculated from the Rietveld model.

These collective results have shown that use of integrated theory and experiment have allowed us to arrive at a correct structural solution for SNL-A. Specifically, Rietveld structure refinement, Density Functional Theory optimization, and solid state ^{133}Cs and ^{29}Si NMR, were all necessary to obtain the most accurate description of a complex phase (of which single crystals of suitable size cannot be grown) which has a unit cell containing 24 crystallographically unique atoms.

Finally, leach tests and irradiation experiments showed SNL-A to be extremely resistant to both structural damage and Cs loss by either method. These results suggest that SNL-A is a viable silicotitanate phase for ceramic waste forms, such as for sequestration of ^{137}Cs. Furthermore, DFT total energy calculations showed the cohesive energy for *Cc* SNL-A to be lower, and thus energetically favorable within the constraints of the model, relative to the high temperature *C2/c* PNNL polymorph. Since the SNL-A polymorph of $Cs_2TiSi_6O_{15}$ is favored under hydrothermal synthesis conditions ($\leq$ 200 °C) and the PNNL polymorph is favored by high temperature routes, it is expected that kinetics rather than thermodynamics dictate the formation of these two phases. For future work, we will investigate the relative stability of the two $Cs_2TiSi_6O_{15}$ polymorphs using high temperature oxide melt calorimetry[51], where the enthalpies of formation from oxides for these phases can be determined.

Acknowledgements

This work was supported by the U.S. DOE under contract DE-AC04-94AL85000 (Sandia National Laboratories).

All authors thank the DOE Environmental Management Science Program (EMSP) for funding for this work under separate grants for the University of Michigan and SNL (EMSP grant DE-FG07-97ER45652 at the University of Michigan; project # 27601 at SNL).

We thank Dr. Todd Alam at Sandia National Laboratories for the preliminary NMR spectroscopy experiments, and M. Lou Balmer (PNNL), Yali Su (PNNL), Alex Navrotsky (U.C. Davis) and Hongwu Xu (U. C. Davis) for helpful discussions.

Table 1. Comparison of agreement indices for the three models.

Model	R_{Bragg}	R_p	R_{wp}	χ^2
Free Rietveld refinement	3.20	11.63	15.56	7.53
Rietveld refinement with Si-O constraint	3.37	11.73	15.69	7.62
DFT model with Cs positions and unit cell fixed by free Rietveld refinement	4.53	12.53	16.37	8.05

Table 2. Crystallographic Data for SNL-A

Chemical Formula	$Cs_2TiSi_6O_{15}$
M(g/mol)	722.2
Crystal System	Monoclinic
Space Group	*Cc* (#9)
a (Å)	12.988 (2)
b (Å)	7.5014 (3)
c (Å)	15.156 (3)
β	105.80 (3)
Volume (Å^3)	1420.8 (7)
Z	4
D_c (g/cm^3)	3.376
λ	Cu $K_{\alpha 1}$, $K_{\alpha 2}$
Geometry	Bragg-Brentano
Range 2θ (°)	5.00 – 100.00
Step size (°)	0.025
Time per step (s)	20
No. free parameters	91
No. of structural parameters	74
No. "independent" reflections	736
Number of soft constraints	24
Minimum FWHM (°)	0.11
R_I (%)	3.37
R_{wp} (%)	15.69
χ^2	7.62

Table 3 Structural parameters for two models.

	Rietveld refinement with Si-O constraints (1.60 (2) Å)			DFT model using unit cell and Cs coordinates from the free Rietveld refinement		
atom	**x (esd)**	**y (esd)**	**z (esd)**	**x**	**y**	**z**
Cs1	0.25970 (fixed)	0.3658 (8)	0.48146 (fixed)	0.25970	0.36710	0.48146
Cs2	0.2832 (3)	0.1337 (8)	0.8030 (3)	0.28440	0.13450	0.80406
Ti	0.539 (1)	0.240 (1)	0.400 (1)	0.53740	0.24215	0.40110
Si1	0.006 (1)	0.068 (2)	0.249 (1)	0.00110	0.07082	0.25206
Si2	0.057 (1)	0.032 (2)	0.563 (1)	0.05177	0.02796	0.56566
Si3	0.084 (1)	0.444 (2)	0.242 (1)	0.08308	0.45208	0.24143
Si4	0.257 (1)	0.113 (2)	0.056 (1)	0.25245	0.12034	0.05332
Si5	0.322 (1)	0.328 (2)	0.241 (1)	0.31768	0.34226	0.24053
Si6	0.484 (1)	0.074 (2)	0.039 (1)	0.47898	0.07257	0.03624
O1	0.000 (2)	0.124 (4)	-0.002 (1)	0.00000	0.13127	0.00000
O2	0.015 (2)	0.282 (3)	0.261 (2)	0.01025	0.28633	0.25821
O3	0.051 (2)	0.499 (5)	0.136 (2)	0.04866	0.50803	0.13532
O4	0.051 (2)	0.004 (5)	0.166 (2)	0.04979	0.00408	0.17055
O5	0.183 (2)	0.043 (4)	0.576 (2)	0.17949	0.04511	0.57225
O6	0.207 (2)	0.376 (4)	0.262 (2)	0.20523	0.38197	0.26171
O7	0.298 (2)	0.230 (5)	0.146 (2)	0.29846	0.22400	0.14911
O8	0.360 (2)	0.032 (3)	0.027 (2)	0.35342	0.03045	0.02647
O9	0.381 (2)	0.516 (4)	0.236 (2)	0.37190	0.52947	0.22141
O10	0.399 (2)	0.246 (4)	0.332 (2)	0.39077	0.24424	0.32800
O11	0.492 (2)	0.288 (3)	0.030 (2)	0.49162	0.28687	0.03043
O12	0.521 (2)	0.022 (3)	0.461 (2)	0.51437	0.01981	0.45538
O13	0.564 (2)	0.472 (3)	0.341 (1)	0.55830	0.47240	0.34501
O14	0.581 (2)	0.112 (3)	0.304 (2)	0.58085	0.11315	0.30808
O15	0.698 (2)	0.255 (3)	0.478 (2)	0.68731	0.25573	0.47277

Table 4. Selected bond angles and distances for SNL-A from the Rietveld refinement with Si-O constraints (1.60 (2) Å).

Atom A	O(x)$_1$	A-O(x)$_1$ bond length (Å) (esd)	O(x)$_2$	O(x)$_1$-A-O(x)$_2$ bond angle (°) (esd)	Atom A	O(x)$_1$	A-O(x)$_1$ bond length (Å) (esd)	O(x)$_2$	O(x)$_1$-A-O(x)$_2$ bond angle (°) (esd)
Ti	O1	1.97 (3)	O10	89.6 (1.5)	**Si3**	O2	1.59 (2)	O3	111.5 (2.1)
	O10	1.84 (3)	O12	93.4 (1.3)		O3	1.59 (2)	O6	104.8 (1.8)
	O12	1.92 (3)	O14	92.4 (1.2)		O6	1.62 (2)	O14	109.0 (1.8)
	O13	2.02 (3)	O14	89.0 (1.3)		O14	1.58 (2)	O2	113.1 (1.8)
	O14	1.95 (3)	O15	90.7 (1.4)		O2		O6	107.7 (1.9)
	O15	2.08 (3)	O1	88.3 (1.3)		O3		O14	110.4 (2.0)
	O1		O12	89.2 (1.4)	**Si4**	O7	1.59 (2)	O8	109.3 (1.8)
	O1		O13	89.4 (1.2)		O8	1.62 (2)	O5	111.0 (1.8)
	O10		O13	88.8 (1.3)		O5	1.60 (2)	O15	114.2 (1.8)
	O10		O14	91.3 (1.4)		O15	1.58 (2)	O7	106.3 (2.1)
	O12		O15	90.7 (1.2)		O7		O5	108.2 (2.3)
	O13		O15	87.1 (1.2)		O8		O15	107.8 (1.9)
Si1	O2	1.61 (2)	O4	111.3 (2.2)	**Si5**	O6	1.64 (2)	O7	108.3 (1.9)
	O4	1.60 (2)	O9	113.7 (2.0)		O7	1.57 (2)	O9	109.7 (2.1)
	O9	1.62 (2)	O13	102.6 (1.7)		O9	1.62 (2)	O1	100.5 (1.8)
	O13	1.58 (2)	O2	110.1 (1.8)		O10	1.58 (2)	O6	108.4 (2.0)
	O2		O9	106.7 (1.6)		O6		O9	106.8 (1.7)
	O13		O4	111.9 (1.8)		O7		O10	122.0 (2.1)
Si2	O5	1.60 (2)	O11	115.6 (1.8)	**Si6**	O8	1.62 (2)	O11	105.3 (1.6)
	O11	1.60 (2)	O1	108.2 (1.8)		O11	1.62 (2)	O3	113.8 (2.2)
	O1	1.58 (2)	O4	110.5 (2.2)		O3	1.59 (2)	O12	109.7 (1.9)
	O4	1.60 (2)	O5	102.1 (1.8)		O12	1.56 (2)	O8	108.8 (1.7)
	O5		O1	113.5 (1.8)		O8		O3	108.2 (1.8)
	O11		O4	106.7 (2.2)		O11		O12	110.8 (2.0)

Cs-O Distances (Å)

Cs1	O(x)	distance	O(x)	distance	**Cs2**	O(x)	distance	O(x)	distance
	O1	3.07 (3)	O9	3.85 (3)		O2	3.30 (3)	O9	3.20 (3)
	O2	3.99 (3)	O10	3.88 (4)		O4	3.33 (3)	O10	3.20 (3)
	O5	3.11 (3)	O11	3.89 (3)		O5	3.40 (3)	O11	3.93 (3)
	O6	3.21 (3)	O12	3.26 (3)		O6	3.82 (3)	O12	3.55 (3)
	O7	3.88 (4)	O14	3.56 (3)		O7	3.66 (4)	O13	3.16 (3)
	O8	3.25 (3)	O15	3.02 (2)		O8	3.36 (3)	O14	3.24 (3)
								O15	3.24 (2)

Table 5.

Comparison of Rings of the PNNL and SNL-A Polymorphs of $Cs_2TiSi_6O_{15}$

Phase [building blocks]	Ring type	Ring polyhedra
SNL-A $Cs_2TiSi_6O_{15}$ (*Cc* polymorph) [$Si(1)O_4$, $Si(2)O_4$, $Si(3)O_4$, $Si(4)O_4$, $Si(5)O_4$, $Si(6)O_4$, TiO_6]	3-ring	Si(2)-Si(4)-Ti
		Si(1)-Si(6)-Ti
	5-ring	Si(2) -Si(1) -Si(5) -Si(4) -Si(6)
		Si(2) -Si(1) -Si(3) -Si(5) -Si(6)
	5-ring	Ti-Si(6)-Si(3) -Si(1) -Si(2)
		Ti-Si(1) -Si(2) -Si(6) -Si(3)
	6-ring	Ti-Si(2) -Si(6) -Ti-Si(3) -Si(1)
	7-ring	Ti-Si(3) -Si (5) -Ti-Si (2) -Si(6) -Si(4)
		Ti-Si(6) -Si (4) -Ti-Si (1) -Si(3) -Si(5)
	8-ring	Si(6)-Si(2)–Si(4)-Si(6)-Si(3)-Si(1)-Si(5)-Si(3)
PNNL $Cs_2TiSi_6O_{15}$[14] (*C2/c* polymorph) [$Si(1)_2O_7$, $Si(2)\,O_4$, $Si(3)\,O_4$, TiO_6]	3-ring	Si(2)-Si(3)-Ti
	5-ring	Si(2)-Si(3)-Si(1)-Si (2)-Si(3)
	5-ring	Ti Si(2) Si(3) $Si(1)_2$
	6-ring	Ti Si(1) Si(3) Ti Si(1) Si(3)
	8-ring	$Si(1)_2$-Si(2) -Si(3) -$Si(1)_2$-Si(3) -Si(2)
	8-ring	Ti-Si(2) -Si(1) -Si (3) -Ti-Si(2) -Si(1) -Si(3)

Table 6. Observed and calculated ^{29}Si NMR shifts and related structural data for SNL-A.

Observed ^{29}Si NMR peak shifts			**^{29}Si NMR peak shifts calculated from DFT model data**			**^{29}Si NMR peak shifts calculated from Rietveld refinement data**		
Si (x)	δ_{obs} (ppm)	Peak integation (% of total)	δ_{calc} (ppm)	Avg. Si(x)-O-Si(y) angle (°)	Si(x)- O-Ti angle (°)	δ_{calc} (ppm)	Avg. Si(x)-O-Si(y) angle (°)	Si(x)- O-Ti angle (°)
Si(1)	-96.8	16.3	-95.1	140	135	-94.9	145	133
Si(4)	-97.8	19.6	-96.0	141	134	-96.2	145	132
Si(2)	-100.2	17.9	-97.7	142	134	-97.5	144	134
Si(5)	-102.4	15.5	-101.6	147	139	-106.9	154	154
Si(6)	-107.3	15.5	-106.5	150	146	-107.1	154	143
Si(3)	-110.0	15.2	-109.6	154	156	-107.8	150	149

Figure Captions

Figure 1. Scanning electron micrographs of SNL-A at 1000x magnification (left) showing the uniformity and purity of the sample; and 3500x magnification (right) illustrating the irregular crystallite shape.

Figure 2. Calculated, observed, and difference profiles for the Rietveld refinement of SNL-A in the *Cc* space group.

Figure 3. Calculated diffraction patterns for the PNNL (top) and SNL-A (bottom) polymorphs of $Cs_2TiSi_6O_{15}$.

Figure 4. View of SNL-A, approximately down the *a*-axis, emphasizing the 5-rings (1Ti, 4Si) and 6-rings (2Ti, 4Si).

Figure 5. View of SNL-A, approximately along (011). This view reveals a 3-ring (1Ti, 3Si), an 8-ring (8Si) and a 7-ring (2Ti, 5Si). The shortest Cs-Cs distances are found in the channels formed by the 7-rings and 8-rings.

Figure 6. View of SNL-A showing the approximately perpendicular layers of 8-rings (8Si) and 5-rings (5Si).

Figure 7. a) ^{133}Cs MAS NMR of SNL-A showing two unique Cs sites in a 1:1 ratio. * indicates spinning side bands. b) ^{29}Si MAS NMR of SNL-A showing 6 unique Si Q^3 (3Si, 1Ti) sites in ~1:1:1:1:1:1 ratio.

Figure 8. View of Cs1 and Cs2 showing coordination environments.

Figure 9. Cohesive energy (eV/primitive cell) as a function of primitive unit cell volume, calculated for the SNL-A *Cc* solution, the SNL-A *C2/c* solution, and the *C2/c* PNNL $Cs_2TiSi_6O_{15}$.

Figure 10. Product consistency test (PCT) leach test for SNL-A showing Cs leach rate as a function of time.

Figure 11. Electron diffraction pattern of SNL-A before and after cumulative radiation dose of 5×102^3 electrons/cm^2. No changes in the electron diffraction pattern resulting from irradiation induced amorphization are observed.

References

1) Wilson, E. K. *Chem. Eng. News* **1997**, 30.
2) Illman, D. L. *Chem. Eng. News* **1993**, 9.
3) Nenoff, T. M.; Thoma, S. G.; Krumhansl, J. L., SAND96-2580: "The Stability and Selectivity of TAM5: A Silicotitanate Molecular Sieve for Radwaste Clean-up," Sandia National Laboratories, 1996.
4) Poojary, D. M.; Cahill, R. A.; Clearfield, A. *Chem. Mater.* **1994**, *6*, 2364.
5) Anthony, R. G.; Phillip, C. V.; Dosch, R. G. *Waste Management* **1993**, *13*, 503.

6) Anthony, R. G.; Dosch, R. G.; Gu, D.; Philip, C. V. *Ind. Eng. Chem. Res.* **1994**, *33*, 2702.

7) Su, Y.; Balmer, M. L.; Wang, L.; Bunker, B. C.; Nenoff, T. M.; Nyman, M.; Navrotsky, A., *"Evaluation of Thermally Converted Silicotitanate Waste Forms"* : Boston, MA, 1998, p 77.

8) Su, Y.; Balmer, M. L.; Bunker, B. C., *"Evaluation of Cesium Silicotitanates as an Alternative Waste Form"* : Boston, MA, 1997, p 457.

9) Xu, H.; Navrotsky, A.; Nyman, M.; Nenoff, T. M. *J. Mater. Res.* **2000**, *15*, 815.

10) Behrens, E. A.; Poojary, D. M.; Clearfield, A. *Chem. Mater.* **1996**, *8*, 1236.

11) Behrens, E. A.; Clearfield, A. *Micropor. Mater.* **1997**, *11*, 65.

12) Balmer, M. L.; Su, Y.; Grey, I. E.; Santoro, A.; Roth, R. S.; Huang, Q.; Hess, N.; Bunker, B. C., *"The Structure and Properties of Two New Silicotitanate Zeolites"* : Boston, MA, 1997, p 449.

13) Balmer, M. L.; Huang, Q.; Wong-Ng, W.; Roth, R. S.; Santoro, A. *J. Sol. State Chem.* **1997**, *130*, 97 .

14) Grey, I. E.; Roth, R. S.; Balmer, M. L. *J. Sol. State Chem.* **1997**, *131*, 38.

15) McCready, D. E.; Balmer, M. L.; Keefer, K. D. *Powder Diffract.* **1997**, *12*, 40.

16) Nyman, M.; Nenoff, T. M.; Gu, B.; Wang, L.; Ewing, R. C. *J. Microporous and Mesoporous Mater.* **submitted 2000.**

17) Nyman, M.; Nenoff, T. M.; Su, Y.; Balmer, M. L.; Navrotsky, A.; Xu, H., *"New Crystalline Silicotitanate (CST) Waste Forms: Hydrothermal Synthesis and Characterization of Cs-Si-Ti-O Phases"* : Boston, MA, 1998, p 71.

18) Li, H.; Tomozawa, M. *J. Non-cryst. Sol.* **1996**, *195*, 188.

19) Mesko, M. G.; Day, D. E. *J. Nucl. Mater.* **1999**, *273*, 27.

20) Su, Y., personal communication.

21) Werner, P. E.; Eriksson, J.; Westdahl, J. *J. Appl. Cryst.* **1985**, *18*, 367.

22) Boultif, A.; Louer, D. *J. Appl. Cryst.* **1991**, *24*, 987.

23) LeBail, A.; Duroy, H.; Fourquet, J. *Mater. Res. Bull.* **1988**, *23*, 447.

24) Rodriguez-Carvajal, J., *"Collected Abstracts of Powder Diffraction Meeting"* : Toulouse, France, 1990, p 127.

25) Altomare, A.; Cascarano, G.; Giacovazzo, C.; Guagliardi, A.; Burla, M. C.; Polidori, G.; Camalli, M. *J. Appl. Cryst.* **1994**, *27*, 435.

26) Farrugia, L. J. *J. Appl. Cryst.* **1999**, *32*, 837.

27) Jouanneaux, A. *CPD Newsletter* **1999**, *21*, 13.

28) LePage, Y. *J. Appl. Cryst.* **1987**, *20*, 264.

29) Kresse, G.; Furthmuller, J. *Comp. Mat. Sci.* **1996**, *6*, 15.

30) Kresse, G.; Hafner, J. *Phys. Rev. B* **1993**, *47*, 558.

31) Kresse, G.; Hafner, J. *Phys. Rev. B* **1994**, *49*, 14251.

32) Kresse, G.; Furthmuller, J. *Phys. Rev. B* **1996**, *54*, 11169.

33) Pulay, P. *Chem. Phys. Lett.* **1980**, *73*, 393.

34) Wood, D. M.; Zunger, A. *J. Phys. A* **1985**, *18*, 1343.

35) Hohenberg, P.; Kohn, W. *Phys. Rev.* **1964**, *136*, 864.

36) Kohn, W.; Sham, L. J. *Phys. Rev.* **1965**, *140*, 1133.

37) Perdew, J. P.; Zunger, A. *Phys. Rev. B* **1981**, *23*, 5048.

38) Ceperley, D. M.; Alder, B. J. *Phys. Rev. Lett.* **1980**, *45*, 566.

39) Balmer, M. L.; Bunker, B. C.; Wang, L. Q.; Peden, C. H. F.; Su, Y. *J. Phys. Chem. B* **1997**, *101*, 9170.

40) Sherriff, B. L.; Grundy, H. D. *Nature* **1988**, 819.

41) Labouriau, A.; Higley, T. J.; Earl, W. L. *J. Phys. Chem.* **1998**, *102*, 2897.

42) Malek, A.; Ozin, G. A.; Macdonald, P. M. *J. Phys. Chem.* **1996**, *100*, 16662.

43) Ahn, M. K.; Iton, L. E. *J. Phys. Chem.* **1991**, *95*, 4496.

44) Yagi, F.; Kanuka, N.; Tsuji, H.; Nakata, S.; Kita, H.; Hattori, H. *Micropor. Mater.* **1997**, *9*, 229.

45) Birch, F. *J. Geophys. Res.* **1978**, *83*, 1257.

46) Bouckaert, L. P.; Smoluchowski, R.; Wigner, E. *Phys. Rev.* **1936**, *50*, 58.

47) Monkhorst, H. J.; Pack, J. D. *Phys. Rev. B.* **1976**, *13*, 5188.

48) Evarestov, R. A.; Smirnov, V. P. *Phys. Stat. Sol.* **1983**, *119*, 9.

49) Wang, L. M.; Wang, S. X.; Ewing, R. C., *"Radiation Effects in Zeolite: Relevance to near-field contamination"* : Las Vegas, NV, 1997, p 772.

50) Wang, L. M.; Wang, S. X.; Gong, W. L.; Ewing, R. C.; Weber, W. J. *Mater. Sci. Eng.* **1998**, *A253*, 106.

51) Navrotsky, A. *Phys. Chem. Miner.* **1997**, *24*, 222.

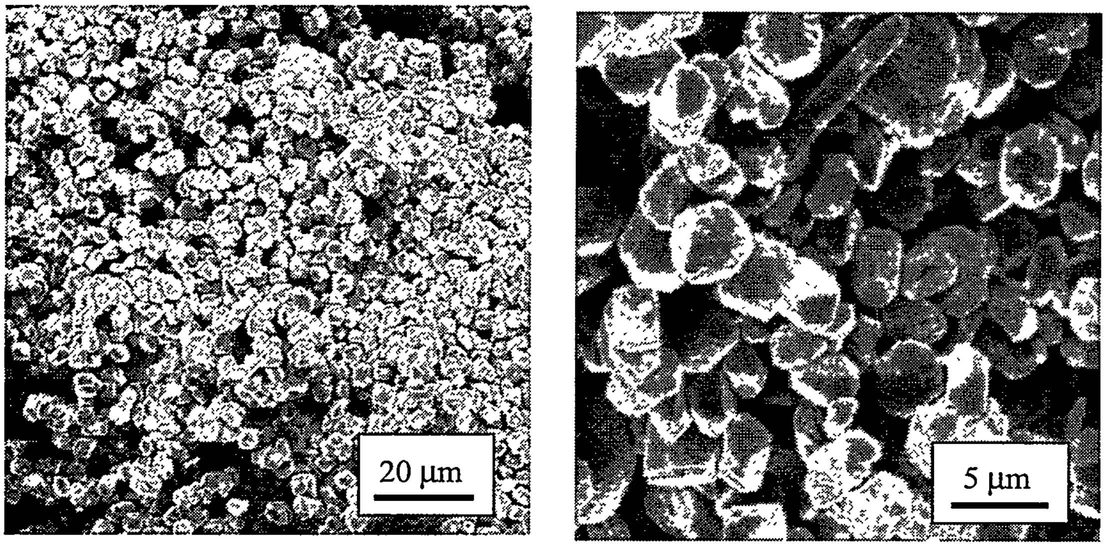
20 μm
5 μm

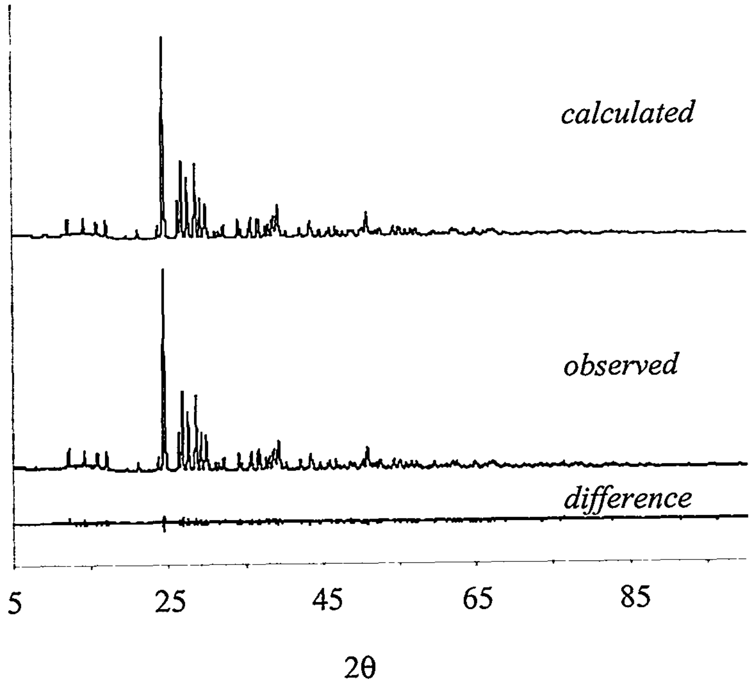
calculated
observed
difference
5
25
45
65
85
2θ

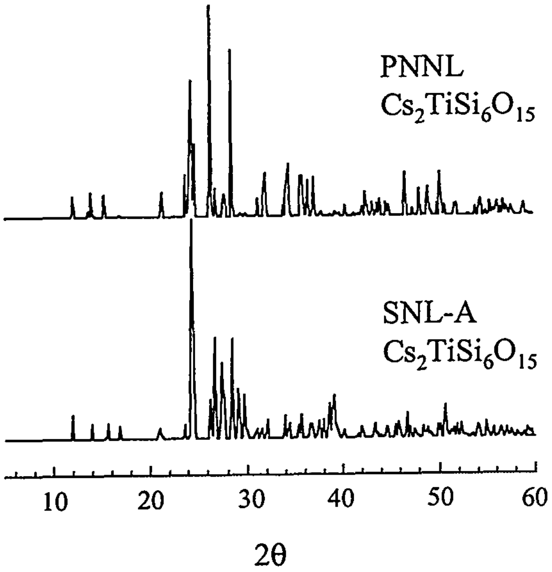
PNNL
$Cs_2TiSi_6O_{15}$
SNL-A
$Cs_2TiSi_6O_{15}$
10
20
30
40
50
60
2θ

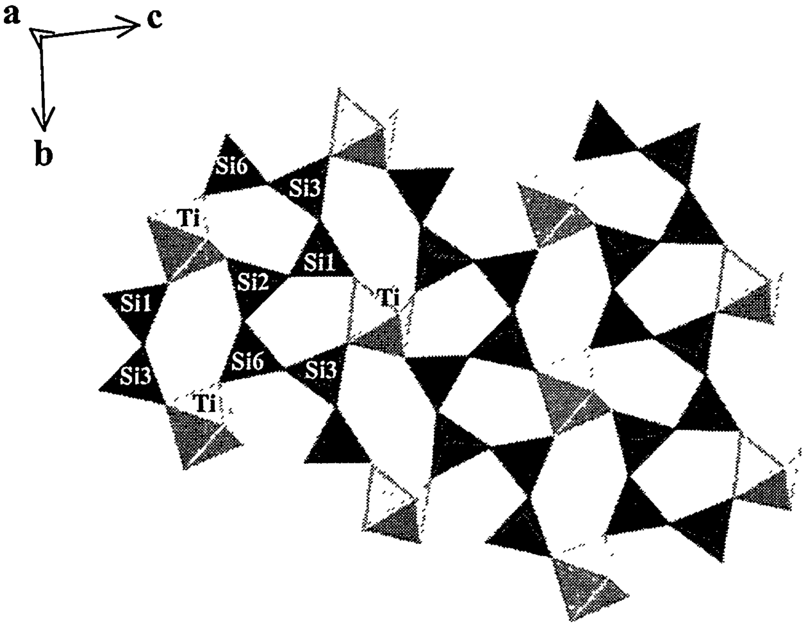
a
c
b
Si6
Si3
Ti
Si1
Si2
Si1
Ti
Si6
Si3
Si3
Ti

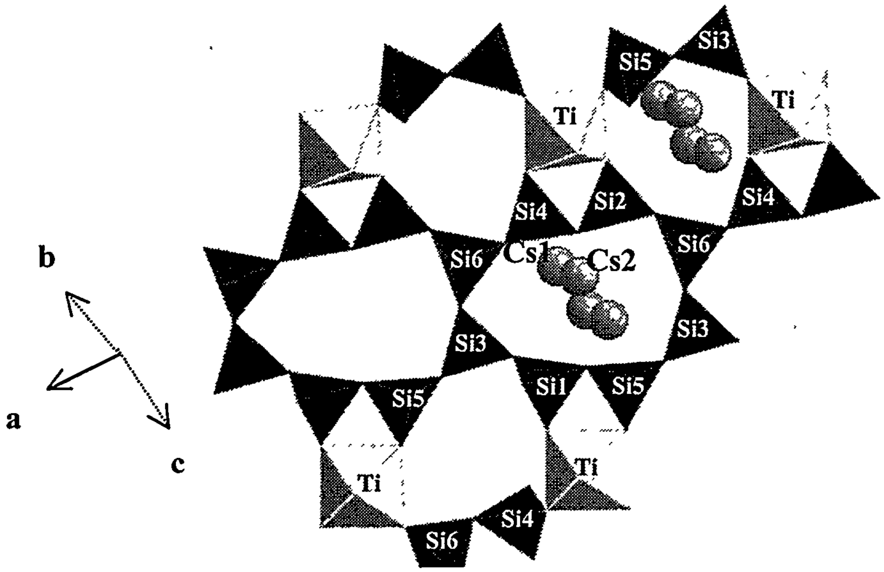
Si5
Si3
Ti
Ti
Si4
Si2
Si4
Si6
Si6
Cs1
Cs2
Si3
Si3
Si5
Si1
Si5
Ti
Ti
Si4
Si6
b
a
c

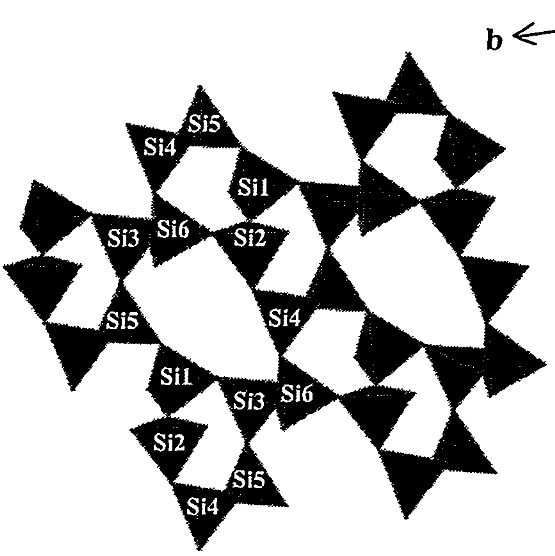
c
b
a
Si5
Si4
Si1
Si3
Si6
Si2
Si5
Si4
Si1
Si3
Si6
Si2
Si5
Si4

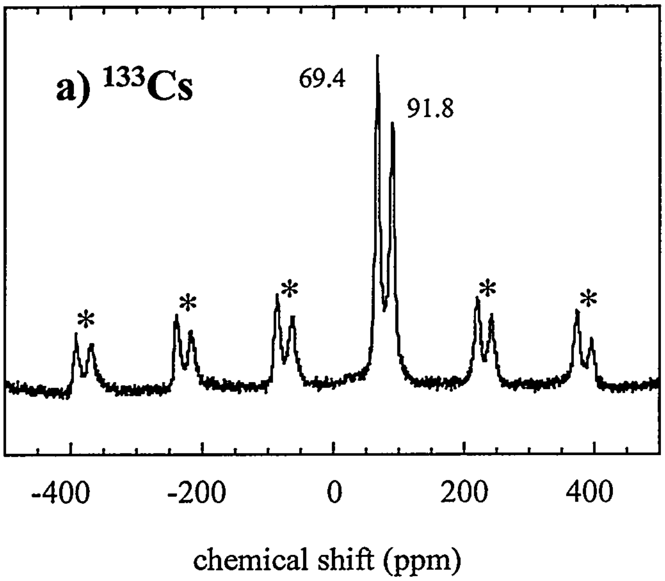
a) ^{133}Cs
69.4
91.8
*
*
*
*
*
-400
-200
0
200
400
chemical shift (ppm)

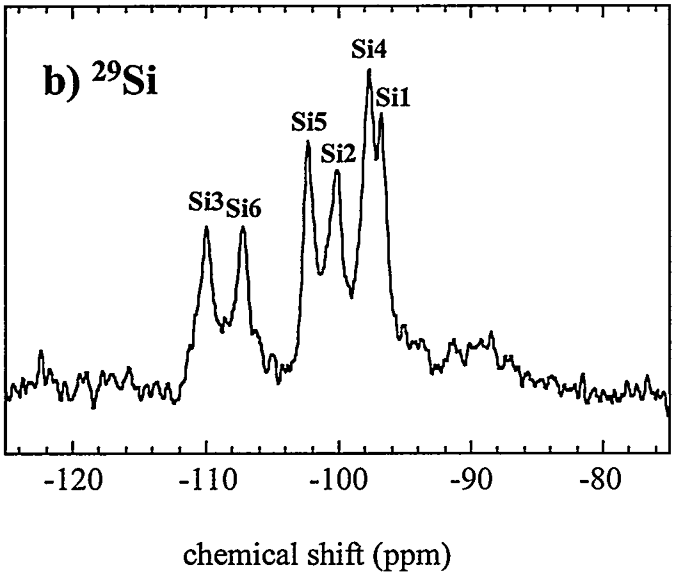
b) ^{29}Si
Si4
Si1
Si5
Si2
Si3
Si6
-120
-110
-100
-90
-80
chemical shift (ppm)

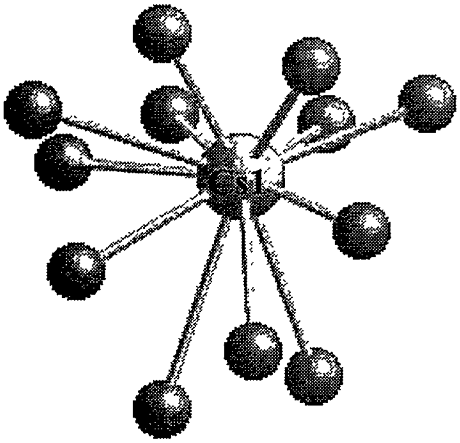
Cs1

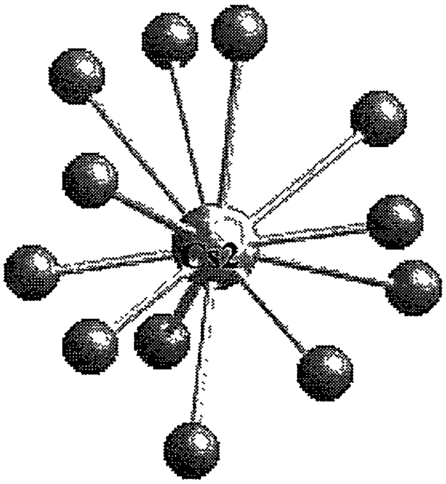
Cs2

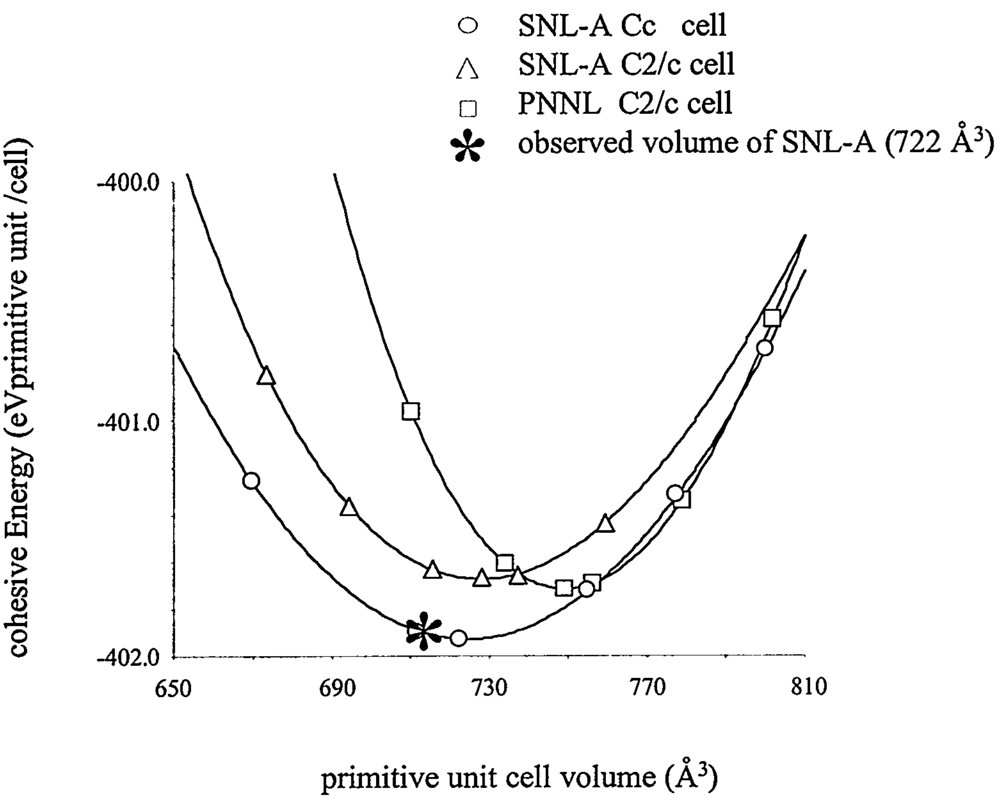
○ SNL-A Cc cell
△ SNL-A C2/c cell
□ PNNL C2/c cell
✻ observed volume of SNL-A (722 Å³)
cohesive Energy (eVprimitive unit /cell)
-400.0
-401.0
-402.0
650
690
730
770
810
primitive unit cell volume (Å³)

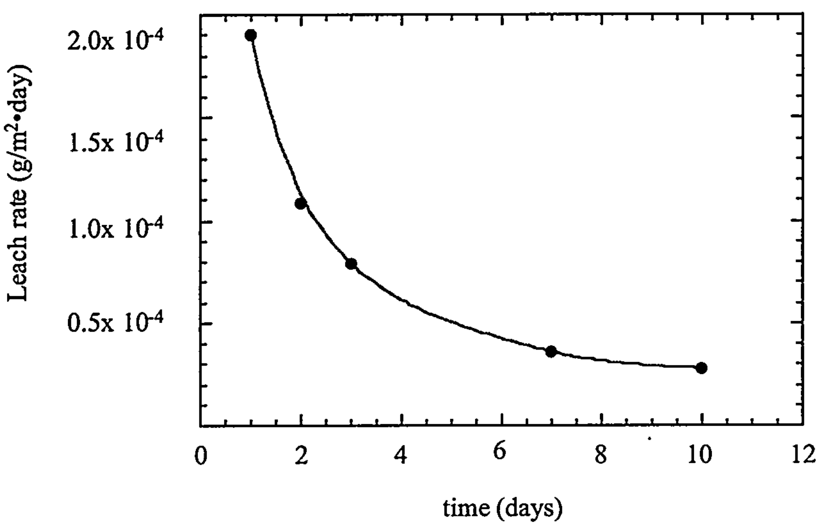
Leach rate (g/m^2•day)
2.0x 10^{-4}
1.5x 10^{-4}
1.0x 10^{-4}
0.5x 10^{-4}
0
2
4
6
8
10
12
time (days)